Fast Polynomial Approximation to Heat Diffusion in Manifolds

Shih-Gu Huang[1(✉)], Ilwoo Lyu[2], Anqi Qiu[3], and Moo K. Chung[1]

[1] University of Wisconsin, Madison, WI, USA
shihgu@gmail.com, mkchung@wisc.edu
[2] Vanderbilt University, Nashville, TN, USA
[3] National University of Singapore, Singapore, Singapore

Abstract. Heat diffusion has been widely used in image processing for surface fairing, mesh regularization and surface data smoothing. We present a new fast and accurate numerical method to solve heat diffusion on curved surfaces. This is achieved by approximating the heat kernel using high degree orthogonal polynomials in the spectral domain. The proposed polynomial expansion method avoids solving for the eigenfunctions of the Laplace-Beltrami operator, which is computationally costly for large-scale surface meshes, and the numerical instability associated with the finite element method based diffusion solvers. We apply the proposed method to localize the sex differences in cortical brain sulcal and gyral curve patterns.

Keywords: Chebyshev polynomials · Diffusion wavelets · Heat diffusion · Laplace-Beltrami operator · Brain cortical surface · Sulcal graph patterns

1 Introduction

Heat diffusion has been widely used in image processing as a form of smoothing and noise reduction starting with Perona and Malik's groundbreaking study [15]. Over the years, the diffusion equation has been solved by various numerical techniques [1–4,17]. In [1,2], the isotropic heat equation was solved by the least squares estimation of the Laplace-Beltrami (LB) operator and the finite difference method (FDM). In [3,4], the heat diffusion was solved iteratively by the discrete estimate of the LB-operator using the finite element method (FEM) and the FDM. However, the FDM is known to suffer numerical instability if the sufficiently small step size is not chosen in the forward Euler scheme. In [3,16], diffusion was solved by expanding the heat kernel as a series expansion of the LB-eigenfunctions. Although the LB-eigenfunction approach avoids the numerical instability associated with the FEM based diffusion solvers [3,4], the computational complexity is very high for large-scale surface meshes.

Motivated by the diffusion wavelet transform [11,12,20] and convolutional neural networks (CNN) [5] on graphs, we propose a new fast and accurate numerical method to solve the heat diffusion on manifolds by expanding the heat kernel using orthogonal polynomials. Taking advantage of recurrence relations of

D. Shen et al. (Eds.): MICCAI 2019, LNCS 11767, pp. 48–56, 2019.
https://doi.org/10.1007/978-3-030-32251-9_6

orthogonal polynomials [14], the computational run time of solving diffusion is substantially reduced. We present three examples of the proposed methods based on the Chebyshev, Hermite and Laguerre polynomials. The proposed method is significantly faster than the LB-eigenfunction approach and FEM based diffusion solvers [3]. As an application, the proposed method is applied to a large number of magnetic resonance images (MRI) to localize the sex differences in the sulcal and gyral patterns of the human brain.

The main contributions of the paper are (1) a novel polynomial scheme to solve diffusion on manifolds, which is faster than the existing numerical schemes while achieving high numerical accuracy, and (2) an innovative way to analyze the sulcal and gyral patterns of the whole brain in a mass univariate fashion.

2 Methods

2.1 Heat Diffusion on Manifolds

Suppose functional data $f \in L^2(\mathcal{M})$, the space of square integrable functions on manifold $\mathcal{M}$ with inner product $\langle f, h\rangle = \int_{\mathcal{M}} f(p)h(p)d\mu(p)$, where $\mu(p)$ is the Lebesgue measure such that $\mu(\mathcal{M})$ is the total area or volume of $\mathcal{M}$. Let Δ denote the LB-operator on $\mathcal{M}$. The isotropic heat diffusion at diffusion time σ on $\mathcal{M}$ with initial condition f is given by

$$\frac{\partial g(p,\sigma)}{\partial \sigma} + \Delta g = 0, \quad g(p, \sigma = 0) = f(p). \tag{1}$$

It has been shown that the convolution of f with heat kernel K_σ is the unique solution of the heat diffusion equation [3]. Let ψ_j be the eigenfunctions of the LB-operator with eigenvalues λ_j, i.e., $\Delta\psi_j = \lambda_j\psi_j$, with $0 = \lambda_0 \leq \lambda_1 \leq \lambda_2 \leq \cdots$. The heat kernel can be expanded by the LB-eigenfunctions with exponential weight $e^{-\lambda\sigma}$ as $K_\sigma(p,q) = \sum_{j=0}^{\infty} e^{-\lambda_j\sigma}\psi_j(p)\psi_j(q)$ [3]. Then, with Fourier coefficients $f_j = \langle f, \psi_j\rangle$, the heat diffusion can be expressed as

$$g(p,\sigma) = K_\sigma * f(p) = \sum_{j=0}^{\infty} e^{-\lambda_j\sigma} f_j\psi_j(p). \tag{2}$$

2.2 Heat Diffusion Using Polynomial Expansion

Consider an orthogonal polynomial basis P_n such as Chebyshev, Hermite and Laguerre polynomials, which is often defined by the following second order recurrence [14],

$$P_{n+1}(\lambda) = (\alpha_n\lambda + \beta_n)P_n(\lambda) + \gamma_n P_{n-1}(\lambda), \quad n \geq 0, \tag{3}$$

with initial conditions $P_{-1}(\lambda) = 0$ and $P_0(\lambda) = 1$ in some interval $[a, b]$. We expand the exponential weight $e^{-\lambda\sigma}$ of the heat kernel as

$$e^{-\lambda\sigma} = \sum_{n=0}^{\infty} c_{\sigma,n}P_n(\lambda), \quad c_{\sigma,n} = \int_a^b e^{-\lambda\sigma}P_n(\lambda)d\mu(\lambda). \tag{4}$$

Table 1. The orthogonal conditions, expansion coefficients and recurrence relations of polynomials. I_n in Chebyshev are the modified Bessel functions of the first kind [14].

Method	Orthogonal conditions	Coefficients $c_{\sigma,n}$	Recurrence relations $\alpha_n,\ \beta_n,\ \gamma_n$
Chebyshev	$\int_{-1}^{1} \frac{T_n(\lambda)T_k(\lambda)}{\sqrt{1-\lambda^2}}d\lambda = \frac{(1+\delta_{n0})\pi}{2}\delta_{nk}$	$e^{-\frac{\lambda_{max}}{2}\sigma}(2-\delta_{n0})$ $\cdot(-1)^n I_n(\lambda_{max}\sigma/2)$	$\frac{2(2-\delta_{n0})}{\lambda_{max}},\ \delta_{n0}-2,\ -1$
Hermite	$\int_{-\infty}^{\infty} H_n(\lambda)H_k(\lambda)e^{-\lambda^2}d\lambda = \sqrt{\pi}2^n n!\delta_{nk}$	$\frac{1}{n!}\left(\frac{-\sigma}{2}\right)^n e^{\frac{\sigma^2}{4}}$	$2,\quad 0,\quad -2n$
Laguerre	$\int_{0}^{\infty} L_n(\lambda)L_k(\lambda)e^{-\lambda}d\lambda = \delta_{nk}$	$\frac{\sigma^n}{(\sigma+1)^{n+1}}$	$\frac{-1}{n+1},\ \frac{2n+1}{n+1},\ \frac{-n}{n+1}$

Using (4), the heat kernel convolution (2) becomes

$$K_\sigma * f = \sum_{n=0}^{\infty} c_{\sigma,n} \sum_{j=0}^{\infty} P_n(\lambda_j) f_j \psi_j. \tag{5}$$

Since $P_n(\lambda)$ is a polynomial of degree n, we have $P_n(\lambda_j)\psi_j = P_n(\Delta)\psi_j$, and

$$K_\sigma * f = \sum_{n=0}^{\infty} c_{\sigma,n} P_n(\Delta) f. \tag{6}$$

The direct computation of $P_n(\Delta) f$ requires the computation of $\Delta f, \cdots, \Delta^n f$, which is costly. Instead, we compute $P_n(\Delta) f$ by the recurrence

$$P_{n+1}(\Delta) f = (\alpha_n \Delta + \beta_n) P_n(\Delta) f + \gamma_n P_{n-1}(\Delta) f, \quad n \geq 0, \tag{7}$$

with initial conditions $P_{-1}(\Delta)f = 0$ and $P_0(\Delta)f = f$. In the numerical implementation, we discretized the LB-operator using the cotan formulation [3,20].

Chebyshev, Hermite and Laguerre Polynomials. We present three examples based on the Chebyshev T_n, Hermite H_n and Laguerre L_n polynomials. The Chebyshev polynomials were used in the diffusion wavelet transform [11,20] and CNN on graphs [5]. Following [11], we shift and scale the Chebyshev polynomials to $\overline{T}_n(\lambda) = T_n\left(\frac{2\lambda}{\lambda_{max}} - 1\right)$ over interval $[0, \lambda_{max}]$, where λ_{max} is the maximum eigenvalue of LB-operator in the numerical implementation. We derived the closed-form expressions of the expansion coefficients $c_{\sigma,n}$ for $\overline{T}_n$, H_n and L_n using the orthogonal conditions (Table 1) [10,14]. The parameters $\alpha_n, \beta_n, \gamma_n$ in the recurrence relations (3) and (7) for $\overline{T}_n$, H_n and L_n are also given in Table 1.

Figure 1 is an illustration of the heat diffusion of the left hippocampus surface mesh coordinates ($\sigma = 1.5$, $m = 100$). The reconstruction error is measured by the mean squared error (MSE) (measured in voxel width squared) between the polynomial expansion method and the original surface mesh. Since the Chebyshev expansion method converges the fastest with the smallest error in various surface meshes, it will be used through the paper but other polynomial methods can be similarly applicable. The MATLAB code for generating Fig. 1 is given in http://www.stat.wisc.edu/~mchung/chebyshev.

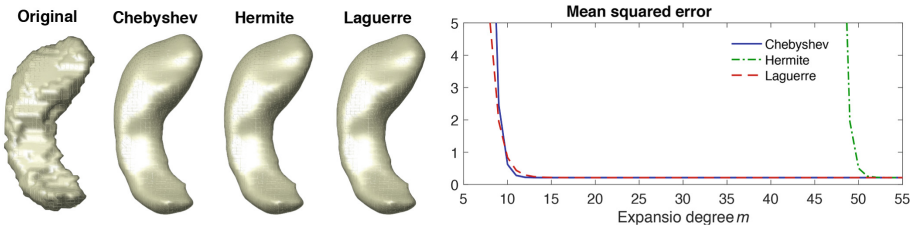

Fig. 1. Left: left hippocampus surface and heat diffusion with $\sigma = 1.5$ using the Chebyshev, Hermite and Laguerre polynomial expansion methods with degree $m = 100$. Right: MSE between the original surface mesh and the polynomial expansion methods for different m. The Chebyshev method converges the fastest in general.

Iterative Convolution. One can obtain diffusion related multiscale features at different time points by iteratively performing heat kernel smoothing. Instead of applying the polynomial expansion method separately for each σ, the computation can also be done quickly by the iterative heat kernel convolution [3]

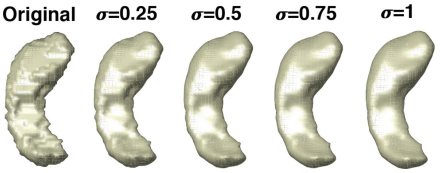

Fig. 2. Sequential application of Chebyshev expansion method with $\sigma = 0.25$ four times.

$$K_{\sigma_1+\sigma_2+\cdots+\sigma_m} * f = K_{\sigma_1} * K_{\sigma_2} \cdots * K_{\sigma_m} * f.$$

For example, if we compute $K_{0.25} * f$, then $K_{0.5} * f$ is simply computed as two repeated kernel convolution $K_{0.25} * (K_{0.25} * f)$, and diffusion with much larger diffusion time can be done similarly. Figure 2 displays heat diffusion with $\sigma = 0.25$, 0.5, 0.75 and 1 realized by iteratively applying the Chebyshev expansion method with $\sigma = 0.25$ sequentially four times.

2.3 Validation

We compared the Chebyshev expansion method against the FEM based diffusion solver [4] and the LB-eigenfunction approach [3] on the unit spheres with 2562, 10242, 40962 and 163842 mesh vertices. On the unit spheres, the ground truth of heat diffusion can be analytically constructed by the spherical harmonics (SPHARM) [18]. Consider the surface signal consisting of values 1, -1 and 0 (Fig. 3). The signal is represented using the SPHARM with degree 100, which is taken as the initial condition of heat diffusion. The SPHARM representation is taken as the ground truth since its diffusion can be analytically given. Figure 3 shows the result with $\sigma = 0.01$ on the unit sphere with 163842 vertices.

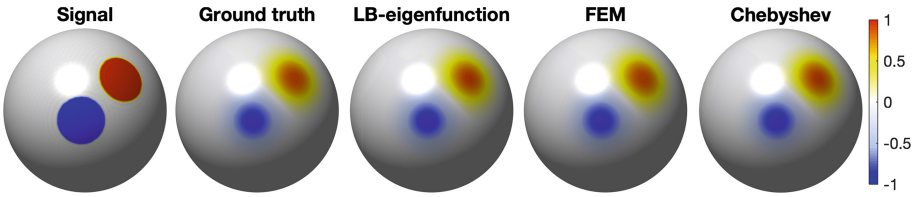

Fig. 3. Signal (initial condition) and ground truth of heat diffusion with $\sigma = 0.01$ are constructed by the SPHARM representation with degree 100. The LB-eigenfunction approach with 210 eigenfunctions, FEM based diffusion solver with 406 iterations, and Chebyshev expansion method with degree 45 have similar accuracy (MSE about 10^{-5}).

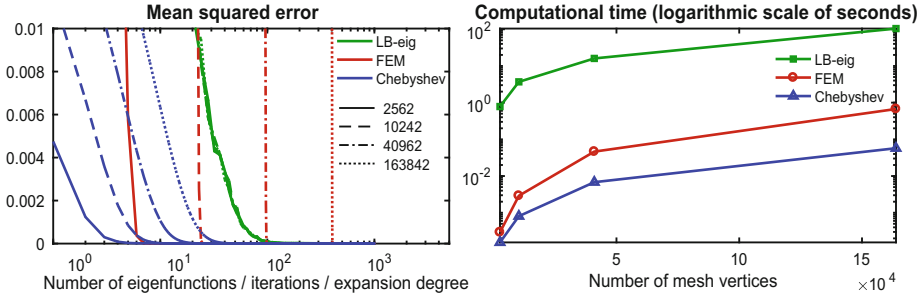

Fig. 4. Left: MSE of the LB-eigenfunction approach, FEM based diffusion solver and Chebyshev expansion method against the ground truth with different number of eigenfunctions, iterations and expansion degree respectively. Unit spheres with 2562, 10242, 40962 and 163842 mesh vertices and fixed $\sigma = 0.01$ were used. Right: computational run time against mesh size at similar accuracy (MSE about 10^{-5}).

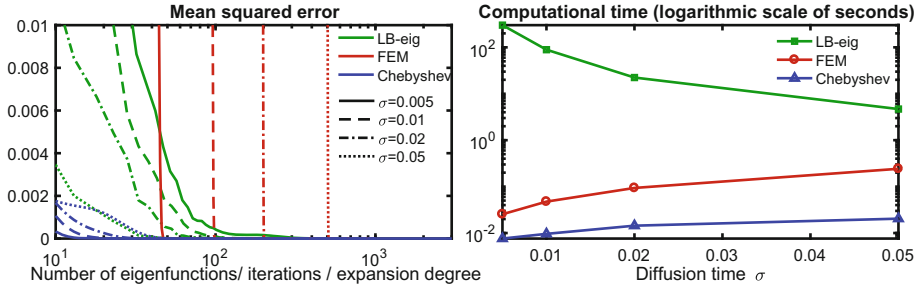

Fig. 5. Left: MSE of the LB-eigenfunction approach, FEM based diffusion solver and Chebyshev expansion method against the ground truth with different number of eigenfunctions, iterations and expansion degree respectively. Diffusion times $\sigma = 0.005$, 0.01, 0.02 and 0.05 and 40962 mesh vertices were used. Right: computational run time versus σ at similar accuracy (MSE about 10^{-7}).

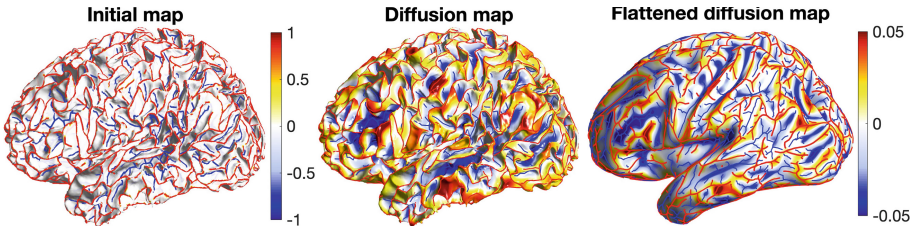

Fig. 6. Left: sulcal (blue) and gyral (red) curves are extracted and displayed on the white matter surface. Middle: heat diffusion using the Chebyshev expansion method with degree 1000 and diffusion time 0.001. Right: diffusion map was flattened to show the pattern of diffusion. (Color figure online)

Run Time over Mesh Sizes. For fixed σ, the FEM based diffusion solver and Chebyshev expansion method need more iterations and higher degree for larger meshes, while the LB-eigenfunction approach is nearly unaffected by the mesh sizes (Fig. 4-left). Since there is a trade-off between the accuracy and computational run time, we fixed the numerical accuracy with MSE at around 10^{-5} and compared the run time (Fig. 4-right).

Run Time over Diffusion Times. For fixed mesh resolution, the FEM based diffusion solver and Chebyshev expansion method need more iterations and higher degree for larger σ, while the LB-eigenfunction approach requires less number of eigenfunctions (Fig. 5-left). Figure 5-right displays the computational run time versus σ with similar MSE of about 10^{-7}.

From Figs. 4 and 5, in terms of reconstruction error, the LB-eigenfunction method is the slowest. The polynomial approximation method is up to twelve times faster than the FEM method.

3 Application

Preprocessing. We used the T1-weighted MRI dataset consisting of 268 females and 176 males collected as the subset of the Human Connectome Project [21]. The MRI data underwent image preprocessing including gradient distortion correction, skull-stripping, bias field correction, nonlinear image registration and white matter and pial surface mesh extractions in FreeSurfer [9]. The automatic sulcal curve extraction method [13] was used to detect concave regions (sulcal fundi) along which sulcal curves are traced. Sulcal points were determined by the line simplification method [7] that denoises the sulcal regions without significant loss of morphological details. A partially connected graph was constructed by the sulcal points, where edge weights are assigned based on geodesic distances. Finally, the sulcal curves were traced over the graph by the Dijkstra's algorithm [6]. Similarly, we extended the same method to the gyral curve extraction by finding convex regions (Fig. 6).

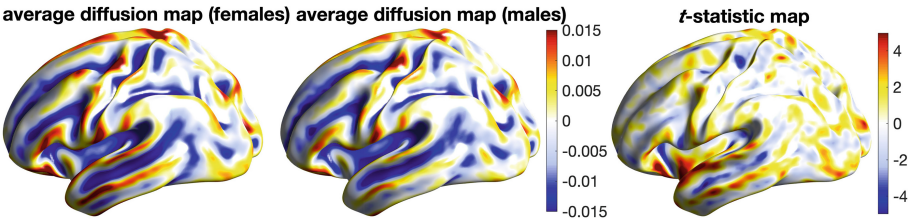

Fig. 7. Left and middle: average diffusion maps of 268 females and 176 males displayed on the average surface template. Right: t-statistic map shows localized sulcal and gyral pattern differences (female-male) thresholded at -4.96 and 4.96 (uncorrected p-value of 10^{-6}).

Diffusion Maps. The sulcal and gyral curves are represented as graphs embedded on the brain surface meshes. It is difficult to establish the precise mapping between curves across subjects. Thus, we applied the proposed method to smooth out sulcal and gyral curves. The gyral curves are assigned value 1, and sulcal curves are assigned value -1. All other parts of surface mesh vertices are assigned value 0 (Fig. 6). The difference in the initial temperature produces heat gradient. We used the Chebyshev expansion method with diffusion time $\sigma = 0.001$ and expansion degree $m = 1000$. On average, the construction of the discrete LB-operator took 5.8 s, and the Chebyshev expansion method took 3.2 s resulting in a total run time of 9 s per subject in a computer. The diffusion maps were subsequently used in localizing the regions of the brain that differentiates male and female differences.

Statistical Analysis. The average diffusion maps of females and males in Fig. 7 show major differences in the temporal lobe among other regions, which is responsible for processing sensory input into derived meanings for the appropriate retention of visual memory, language comprehension, and emotion association [19]. The two-sample t-statistic map (female-male) was constructed on the diffusion maps (max. t-stat. 7.02, min. t-stat. -6.5). The multiple comparisons are corrected using the false discovery rate at 0.05 via the Benjamini-Hochberg procedure [8]. t-statistic values larger than 2.75 and smaller than -2.75 are considered as significant (red and blue regions).

4 Conclusion

In this paper, we proposed a new fast and accurate numerical method to solve heat diffusion on curved surfaces by expanding the heat kernel in the spectral domain by orthogonal polynomials. The proposed polynomial expansion method speeds up the computation significantly compared to existing numerical schemes. The proposed method was applied in the sulcal and gyral curve pattern analysis.

The proposed polynomial method can be applied to multiscale shape analysis via the iterative kernel convolution. The method can be further extended to any

arbitrary domain without much computational bottlenecks. Thus, the method can be easily applicable to large-scale images where the existing methods may not be applicable without additional computational resources, such as 3D volumetric meshes [22]. These are left as future studies.

Acknowledgements. This study was funded by NIH Grant R01 EB022856. We would like to thank Won Hwa Kim of University of Texas Arlington and Vikas Singh of University of Wisconsin-Madison for providing valuable discussions on the diffusion wavelets.

References

1. Andrade, A., et al.: Detection of fMRI activation using cortical surface mapping. Hum. Brain Mapp. **12**, 79–93 (2001)
2. Cachia, A., et al.: A primal sketch of the cortex mean curvature: a morphogenesis based approach to study the variability of the folding patterns. IEEE Trans. Med. Imaging **22**, 754–765 (2003)
3. Chung, M.K., Qiu, A., Seo, S., Vorperian, H.K.: Unified heat kernel regression for diffusion, kernel smoothing and wavelets on manifolds and its application to mandible growth modeling in CT images. Med. Image Anal. **22**, 63–76 (2015)
4. Chung, M.K., Worsley, K.J., Robbins, S., Evans, A.C.: Tensor-based brain surface modeling and analysis. In: IEEE Conference on Computer Vision and Pattern Recognition (CVPR), vol. I, pp. 467–473 (2003)
5. Defferrard, M., Bresson, X., Vandergheynst, P.: Convolutional neural networks on graphs with fast localized spectral filtering. In: Advances in Neural Information Processing Systems, pp. 3844–3852 (2016)
6. Dijkstra, E.W.: A note on two problems in connexion with graphs. Numer. Math. **1**, 269–271 (1959)
7. Douglas, D.H., Peucker, T.K.: Algorithms for the reduction of the number of points required to represent a digitized line or its caricature. Cartographica Int. J. Geograph. Inf. Geovisualization **10**, 112–122 (1973)
8. Genovese, C.R., Lazar, N.A., Nichols, T.: Thresholding of statistical maps in functional neuroimaging using the false discovery rate. NeuroImage **15**, 870–878 (2002)
9. Glasser, M.F., et al.: The minimal preprocessing pipelines for the Human Connectome Project. NeuroImage **80**, 105–124 (2013)
10. Gradshteyn, I.S., Ryzhik, I.M.: Table of Integrals, Series, and Products, 7th edn. Academic, San Diego (2007)
11. Hammond, D.K., Vandergheynst, P., Gribonval, R.: Wavelets on graphs via spectral graph theory. Appl. Comput. Harmonic Anal. **30**, 129–150 (2011)
12. Kim, W.H., Pachauri, D., Hatt, C., Chung, M.K., Johnson, S., Singh, V.: Wavelet based multi-scale shape features on arbitrary surfaces for cortical thickness discrimination. In: Advances in Neural Information Processing Systems, pp. 1241–1249 (2012)
13. Lyu, I., Kim, S., Woodward, N., Styner, M., Landman, B.: TRACE: a topological graph representation for automatic sulcal curve extraction. IEEE Trans. Med. Imaging **37**, 1653–1663 (2018)
14. Olver, F.W.J., Lozier, D.W., Boisvert, R.F., Clark, C.W.: NIST Handbook of Mathematical Functions. Cambridge University Press, Cambridge (2010)

15. Perona, P., Malik, J.: Scale-space and edge detection using anisotropic diffusion. IEEE Trans. Anal. Mach. Intell. **12**, 629–639 (1990)
16. Reuter, M.: Hierarchical shape segmentation and registration via topological features of Laplace-Beltrami eigenfunctions. Int. J. Comput. Vision **89**, 287–308 (2010)
17. Seo, S., Chung, M.K., Vorperian, H.K.: Heat Kernel smoothing using Laplace-Beltrami eigenfunctions. In: Jiang, T., Navab, N., Pluim, J.P.W., Viergever, M.A. (eds.) MICCAI 2010. LNCS, vol. 6363, pp. 505–512. Springer, Heidelberg (2010). https://doi.org/10.1007/978-3-642-15711-0_63
18. Shen, L., Chung, M.: Large-scale modeling of parametric surfaces using spherical harmonics. In: Third International Symposium on 3D Data Processing, Visualization and Transmission (3DPVT), pp. 294–301 (2006)
19. Smith, B., et al.: The OBO foundry: coordinated evolution of ontologies to support biomedical data integration. Nat. Biotechnol. **25**, 1251 (2007)
20. Tan, M., Qiu, A.: Spectral Laplace-Beltrami wavelets with applications in medical images. IEEE Trans. Med. Imaging **34**, 1005–1017 (2015)
21. Van Essen, D.C., et al.: The human connectome project: a data acquisition perspective. NeuroImage **62**, 2222–2231 (2012)
22. Wang, G., Zhang, X., Su, Q., Shi, J., Caselli, R.J., Wang, Y.: A novel cortical thickness estimation method based on volumetric Laplace-Beltrami operator and heat kernel. Med. Image Anal. **22**, 1–20 (2015)